


## Mechanistic insight into acrylate metabolism and detoxification in marine dimethylsulfoniopropionate-catabolizing bacteria

Peng Wang<sup>a,1</sup>, Hai-Yan Cao<sup>a,1</sup>, Xiu-Lan Chen<sup>a</sup>, Chun-Yang Li<sup>a</sup>, Ping-Yi Li<sup>a</sup>, Xi-Ying Zhang<sup>a</sup>,  
Qi-Long Qin<sup>a</sup>, Jonathan D. Todd<sup>c</sup>, Yu-Zhong Zhang<sup>a,b</sup> \* 

<sup>a</sup> Marine Biotechnology Research Center, State Key Laboratory of Microbial Technology, Shandong University, Jinan 250100, China

<sup>b</sup> Laboratory for Marine Biology and Biotechnology, Qingdao National Laboratory for Marine Science and Technology, Qingdao, China

<sup>c</sup> School of Biological Sciences, University of East Anglia, Norwich Research Park, Norwich NR4 7TJ, UK.

<sup>1</sup>P. W and H-Y. C contributed equally to this work.

\* Corresponding author: Yu-Zhong Zhang, State Key Laboratory of Microbial Technology, Shandong University, Jinan 250100, P. R. China. Tel: +86-531-88364326; Fax: +86-531-88564326. E-mail: zhangyz@sdu.edu.cn

This article has been accepted for publication and undergone full peer review but has not been through the copyediting, typesetting, pagination and proofreading process which may lead to differences between this version and the Version of Record. Please cite this article as an 'Accepted Article', doi: 10.1111/mmi.13727

This article is protected by copyright. All rights reserved.

## Summary

Dimethylsulfoniopropionate (DMSP) cleavage, yielding dimethyl sulfide (DMS) and acrylate, provides vital carbon sources to marine bacteria, is a key component of the global sulfur cycle and affects atmospheric chemistry and potentially climate. Acrylate and its metabolite acryloyl-CoA are toxic if allowed to accumulate within cells. Thus, organisms cleaving DMSP require effective systems for both the utilization and detoxification of acrylate. Here, we examine the mechanism of acrylate utilization and detoxification in Roseobacters. We propose propionate-CoA ligase (PrpE) and acryloyl-CoA reductase (AcrI) as the key enzymes involved and through structural and mutagenesis analyses, provide explanations of their catalytic mechanisms. In most cases, DMSP lyases and DMSP demethylases (DmdAs) have low substrate affinities, but AcrIs have very high substrate affinities, suggesting that an effective detoxification system for acrylate catabolism exists in DMSP-catabolizing Roseobacters. This study provides insight on acrylate metabolism and detoxification and a possible explanation for the high  $K_m$  values that have been noted for some DMSP lyases. Since acrylate/acryloyl-CoA is probably produced by other metabolism, and AcrI and PrpE are conserved in many organisms across all domains of life, the detoxification system is likely relevant to many metabolic processes and environments beyond DMSP catabolism.

## Introduction

Dimethylsulfoniopropionate (DMSP) is one of earth's most abundant organosulfur molecules with  $\sim 10^3$  Tg produced each year by marine phytoplankton and, as recently shown, by bacteria (Kiene, 2000, Curson *et al.*, 2017). In the ocean's surface, DMSP can account for  $\sim 10\%$  of fixed carbon (Kiene, 2000, Archer *et al.*, 2001, Simo *et al.*, 2002). DMSP also has important roles in global sulfur cycling (Sievert *et al.*, 2007) and as chemoattractant (Seymour *et al.*, 2010). Via microbial DMSP catabolism, it provides microbial communities with key carbon, reduced sulfur and energy sources (Curson *et al.*, 2011b). Much of the environmental DMSP is taken up by marine bacteria and degraded via a demethylation pathway or a cleavage pathway (Malmstrom *et al.*, 2004, Curson *et al.*, 2011b, Wang *et al.*, 2015). In the cleavage pathway, DMSP is cleaved by DMSP lyases to yield  $\sim 300$  Tg of acrylate and dimethyl sulfide (DMS), an important gas with roles in atmospheric chemistry and potentially

climate (Curson *et al.*, 2011b, Kiene, 2000). Acrylate, which can represent 10-15% of the total carbon in coral exudates (Tapiolas *et al.*, 2010), is also an important carbon source in marine environment. Many marine bacteria that cleave DMSP subsequently metabolise the product acrylate as a carbon source for growth (Yoch, 2002, Todd *et al.*, 2010, Curson *et al.*, 2011a, Curson *et al.*, 2014). However, acrylate is toxic and is further converted into other intracellular toxic compounds, such as the electrophile acryloyl-CoA that attacks sulfhydryl groups, which are detrimental to bacteria (Todd *et al.*, 2012, Clayden *et al.*, 2001). Therefore, acrylate-utilizing organisms require systems in place to detoxify acrylate and its metabolites.

Nearly all reported DMSP-catabolizing bacteria are Proteobacteria, comprising  $\alpha$ -,  $\gamma$ -,  $\beta$ -,  $\delta$ - and  $\epsilon$ -proteobacterial classes. Amongst these, the ability to catabolise DMSP is frequently found in  $\gamma$ -proteobacteria, including some Oceanospirillales, but most notably, the abundant marine  $\alpha$ -proteobacterial Roseobacters (Curson *et al.*, 2011b). Recently, SAR11  $\alpha$ -proteobacteria (order Pelagibacterales), which are the most abundant heterotrophic bacteria in the oceans, were shown to both cleave and demethylate DMSP (Sun *et al.*, 2016). There are many studies of microbial DMSP cleavage and demethylation, but only two detailed reports of acrylate utilization in DMSP-catabolizing bacteria, those being *Halomonas* HTNK1 (an oceanospirillales) and *Ruegeria pomeroyi* DSS-3 (a Roseobacter) (Todd *et al.*, 2010, Reisch *et al.*, 2013, Curson *et al.*, 2014). Two different pathways for acrylate utilization and detoxification were proposed, the AcuN-AcuK pathway and the PrpE-AcuI pathway, which use the acryloyl-CoA transferase (AcuN) and acryloyl-CoA hydratase (AcuK) or the propionate-CoA ligase (PrpE) and acryloyl-CoA reductase (AcuI) enzymes, respectively, as the key enzymes (Todd *et al.*, 2010, Reisch *et al.*, 2013).

In *Halomonas* HTNK1, it is proposed, based on genetics, that acrylate is first hydrated by the acryloyl-CoA transferase (AcuN) and acryloyl-CoA hydratase (AcuK) enzymes yielding 3-hydroxypropionate (3-HP), which is further oxidized to malonate-semialdehyde by the alcohol dehydrogenase DddA. After that, malonate-semialdehyde is decarboxylated by DddC, an aldehyde dehydrogenase, to form acetyl-CoA, which is finally metabolized via the tricarboxylic acid (TCA) cycle (Fig. 1A) (Todd *et al.*, 2010). The key enzymes in this pathway are AcuN and AcuK, which complete the initial steps in this pathway. The AcuN of *Halomonas* HTNK1 belongs to the Class III acyl-CoA transferase superfamily (Pfam ID:

PF02515) and the AcuK of *Halomonas* HTNK1 belongs to the crotonase superfamily (Pfam ID: PF00378) (Elssner *et al.*, 2001, Todd *et al.*, 2010). In the proposed pathway, AcuN first transfers CoA from an acyl-CoA donor to acrylate to produce acryloyl-CoA, and then AcuK acts as an acryloyl-CoA hydratase to produce 3HP-CoA, which would serve as the acyl-CoA donor for AcuN to produce 3-HP ( Todd *et al.*, 2010).

The PrpE-AcuI pathway was proposed in *R. pomeroyi* DSS-3 (DSS-3) (Reisch *et al.*, 2013, Todd *et al.*, 2012) (Fig. 1B). In DSS-3, acrylate is catalyzed by propionate-CoA ligase (PrpE) to generate the cytotoxic electrophile acryloyl-CoA, which is further reduced to less harmful propionate-CoA by acryloyl-CoA reductase (AcuI). Propionate-CoA is finally metabolized via the methylmalonyl-CoA pathway (Fig. 1B) (Reisch *et al.*, 2013). AcuI is believed to be responsible for the detoxification of acrylate (Herrmann *et al.*, 2005, Curson *et al.*, 2014). Consistent with this, an *R. pomeroyi acuI* mutant loses the ability to use acrylate as a sole carbon source and becomes hypersensitive to this metabolite (Todd *et al.*, 2012). This suggests that the PrpE-AcuI pathway predominates in acrylate utilization and detoxification in *R. pomeroyi*, and perhaps other Roseobacters that contain *prpE* and *acuI* genes. The PrpE of DSS-3 belongs to the adenylate-forming superfamily (Reisch *et al.*, 2013), sharing 51% and 45% sequence identities to *Homo sapiens* mitochondrial and *Escherichia coli* PrpEs, respectively. The AcuI of DSS-3 is a homolog of *E. coli* YhdH (53%), which is an NADPH-dependent enzyme of the medium chain reductase/dehydrogenase (MDR) family that catalyzes the reduction of acryloyl-CoA to propionyl-CoA (Reisch *et al.*, 2013, Asao & Alber, 2013).

With acrylate being an important marine carbon source that can be converted into other intracellular toxic compounds, it is of interest to explain the molecular mechanisms for acrylate utilization and detoxification. Molecular, biochemical and mechanistic studies are required to understand how the PrpE-AcuI enzymes function to metabolise and detoxify acrylate. Our study supports the notion that the PrpE-AcuI pathway is the key acrylate metabolic and detoxification pathway in DMSP-catabolizing Roseobacters. We verify the function of the PrpE and AcuI enzymes in three typical DMSP-catabolizing Roseobacters, namely *R. pomeroyi* DSS-3 isolated from a marine electroactive biofilm (Vandecastelaere *et al.*, 2008), *R. lacuscaerulensis* ITI\_1157 (ITI\_1157) isolated from the Blue Lagoon

(Petursdottir & Kristjansson, 1997) and *Dinoroseobacter shibae* DFL 12 (DFL 12) isolated from dinoflagellates (Biebl *et al.*, 2005). Then, by determining the three-dimensional structures of PrpE from DFL 12 and AcuI from DSS-3, we explain the catalytic mechanisms of PrpE and AcuI using structural and mutagenesis analyses. Finally, based on analyses of the substrate affinities of DMSP lyases, DmdA, PrpE and AcuI enzymes, we suggest an effective detoxification system for acrylate catabolism in DMSP-catabolizing Roseobacters through the PrpE-AcuI pathway. It is helpful to avoid the toxicity of acrylate and its metabolites. Furthermore, because PrpE and AcuI are widespread in marine and terrestrial organisms across all domains of life, the acrylate detoxification mechanism is likely relevant to many metabolic processes and environments.

## Results and discussion

### PrpE-AcuI pathway is widespread and functional in DMSP-catabolizing Roseobacters

Roseobacters are abundant DMSP-catabolizing bacteria in marine environments. To investigate whether DMSP-catabolizing Roseobacters possess the genetic capacity to metabolise acrylate via PrpE-AcuI pathway, we conducted a bioinformatics analysis on sequenced Roseobacters for the presence of the *prpE* and *acuI* genes. We found that 95% of sequenced Roseobacters contained good matches to both *prpE* and *acuI* in the PrpE-AcuI pathway (Fig. S1). Conversely, no sequenced Roseobacters contained AcuN homologues (>50% identity) despite most containing AcuK (Fig. S1). This supports the PrpE-AcuI pathway as the likely acrylate utilization and detoxification pathway in most Roseobacters. The DMSP-catabolizing Roseobacters *R. pomeroyi* DSS-3, *R. lacuscaerulensis* ITI\_1157 and *D. shibae* DFL 12 were chosen as models to further study the transcription and functionality of these pathways because they are the most widely studied DMSP-catabolizing Roseobacters and were isolated from diverse marine environments.

We assayed the transcription of the putative *prpE*, *acuI*, *acuN* and *acuK* genes in DSS-3, ITI\_1157 and DFL 12 (the putative *acuN* genes are <50% identity to the *acuN* gene in *Halomonas* HTNK1, it has the possibility that these DMSP-catabolizing Roseobacters don't contain *acuN*) grown in the presence and absence of DMSP or acrylate using RT-qPCR to imply their *in vivo* function in the degradation of these compounds. As shown in Fig. 2A, the

transcription of the *acuNK*-like genes was low level constitutive irrespective of either DMSP or acrylate. In contrast, the *prpE* and *acuI* transcription was significantly enhanced by both DMSP and acrylate in all three strains, further supporting their active role in the degradation of acrylate and acryloyl-CoA. Furthermore, purified recombinant PrpE and AcuI enzymes from DSS-3, ITI\_1157 and DFL 12 showed significant PrpE and AcuI *in vitro* activities. As shown in Figs. 2B, 2C and S6, the enzymatic assay of PrpE detected the production of acryloyl-CoA compared to the control assay (Fig. 2B and S6) and the enzymatic assay of AcuI detected the reduction of acryloyl-CoA and the production of propionate-CoA compared to the control assay (Fig. 2C and S6). The control assays have the same reaction system as the corresponding enzymatic assays except that PrpE/AcuI was not added.

Our results, together with the fact that a DSS-3 *acuI* mutant is unable to grow on acrylate as sole carbon source and is hypersensitive to acrylate (Reisch *et al.*, 2013, Alcolombri *et al.*, 2014, Todd *et al.*, 2012), indicate that the PrpE-AcuI pathway is widespread in DMSP-catabolizing Roseobacters and is probably required for these abundant marine bacteria to metabolise and/or detoxify acrylate, the product of DMSP lysis. The following work is focused on determining the catalytic mechanisms of PrpE and AcuI to reveal how DMSP-catabolizing Roseobacters metabolize acrylate and avoid the accumulation of toxic acrylate and acryloyl-CoA.

### Overall structure of PrpE

The high sequence identities of the PrpE and AcuI enzymes in sequenced Roseobacters (Fig. S1) suggest that they probably have similar protein structures and function. To study the catalytic mechanism of PrpE in acrylate metabolism, we solved the structures of PrpE from DFL 12 (82% identity to PrpE from DSS-3). Although the crystal structure of apo-PrpE was not obtained, the structure of PrpE in complex with adenosine monophosphate (AMP), acrylate and CoA was determined to a 2.0 Å resolution. PrpE is a monomer in its asymmetric unit within the crystal. Gel filtration analysis showed that PrpE is also a monomer in solution (Fig. 3A). The topological structure of PrpE is similar to those of other acyl- or aryl-CoA synthetases, such as acetyl-CoA synthetase from *Salmonella enterica* (Reger *et al.*, 2007) and 4-chlorobenzoate CoA synthetase from *Alcaligenes sp.* AL3007 (Gulick *et al.*, 2004). PrpE contains an N-terminal domain (N-domain) and a C-terminal domain (C-domain) (Fig. 3B).

The N-domain contains 492 residues of the N-terminus, which form two  $\beta$ -sheets of seven strands (sheet 1 and sheet 2) and a  $\beta$ -sheet of five strands (sheet 3). The  $\beta$ -sheets 1 and 2 are arranged parallel to each other and sandwich eight helices between them (Fig. 3B). The C-domain contains 138 residues of the C-terminus, which form a three-stranded  $\beta$ -sheet (sheet 4) with helices on its face. Although similar to the structure of the acetyl-CoA synthetase (PDB code: 2P2F, identity: 39%) from the same protein family, this is the first structure for PrpE.

### **Overall structure of AcuI**

The crystallized AcuI is from DSS-3. The crystal structures of apo-AcuI (Fig. 3C) and of AcuI in complex with NADPH (Fig. 3D) were determined to 2.3 Å and 1.7 Å resolution, respectively. The overall structures of the two structures are similar, with a root-mean-square deviation (rmsd) of 0.313 Å, indicating that the binding of NADPH had little impact on the overall structure of AcuI. Both structural and gel filtration analyses showed that AcuI forms intimate dimers (Fig. 3A, C). The AcuI dimer is assembled through a large interface and mainly locked by two antiparallel strand-strand interactions (Fig. 3C). The AcuI monomer contains 330 residues. It contains a typical rossmann fold which binds the NADPH cofactor (Fig. 3D). The structure of *R. pomeroyi* AcuI is very similar to that of YhdH (PDB code: 3NX4) from *E. coli* (Sulzenbacher *et al.*, 2004), which is expected since they share 53 % amino acid identity and are both acryloyl-CoA reductases (Asao & Alber, 2013, Todd *et al.*, 2012). Both structures lack Zn co-factors, their topological structures are alike and the key residues are identical (Fig. S2). These findings suggest that AcuI enzymes, not only those within DMSP-catabolizing Roseobacters, may have similar structures, molecular characteristics and catalytic mechanisms -e.g., those from *R. pomeroyi*, *E. coli* and even *Drosophila* (52% to DSS-3 AcuI).

### **The catalytic mechanism of PrpE for acryloyl-CoA ligation**

PrpE belongs to the adenylate-forming superfamily and has sequence similarity with other acyl-CoA ligases, e.g., *S. enterica* acetyl-CoA synthetase (PDB code: 2P2F, 38% identity). Acyl-CoA ligases in the adenylate-forming superfamily catalyze a typical two-step reaction. In the initial half-reaction, an acyl-AMP intermediate is formed and a pyrophosphate is released from ATP. In the second half-reaction, an AMP molecule is released from acyl-AMP

and acyl-CoA is formed (Jogl & Tong, 2004, Reger *et al.*, 2007, Gulick *et al.*, 2003). Acyl-CoA ligases usually go through a conformational change from the adenylate-forming conformation to the thioester-forming conformation, in which the C-domain rotates approximately 140° (Reger *et al.*, 2007, Gulick *et al.*, 2003, Jogl & Tong, 2004, Kochan *et al.*, 2009, Hisanaga *et al.*, 2004). Adenylate-forming superfamily enzymes typically contain 10 regions of highly conserved residues that have been named A1-A10 (Marahiel *et al.*, 1997). PrpE also contains these conserved regions (Fig. S3).

Our solved PrpE structure is in the thioester-forming conformation. In this conformation, the A10 region is far away (>27 Å) from the active site (Fig. 4A). To further understand the likely mechanisms of the PrpE reaction, we constructed a series of site-directed mutations to residues within the 10 conserved regions of PrpE based on structural and sequence alignment analyses. Interestingly, the mutation K588A in the A10 region completely abolished the activity of PrpE, indicating that Lys588 is essential for PrpE activity (Fig. 4C). Furthermore, mutations (R493A, R493G, T494A, D496A and D496G) within the linker between the N-domain and the C-domain also reduced the activity of PrpE (Fig. 4A, C). These results suggest that it is most likely that PrpE undergoes a C-terminal rotation in the acryloyl-CoA ligation reaction, just as in the case of other acyl-CoA ligases in the adenylate-forming superfamily (Reger *et al.*, 2007). To study the adenylate-forming conformation of PrpE, we rotated (*in silico*) the C-domain of PrpE according to the structures of the adenylate-forming conformations of yeast acetyl-CoA synthetase (PDB code: 1RY2) and of long-chain fatty acyl-CoA synthetase (PDB code: 1V26) (Fig. 4B). After rotation, PrpE is in the adenylate-forming conformation. In this conformation, the A10 region is relocated into the active site. Furthermore, residues Arg493, Thr494 and Asp496 are on the rotation hinge. Based on structural and mutagenesis analyses and previous studies (Reger *et al.*, 2007, Gulick *et al.*, 2003, Jogl & Tong, 2004, Kochan *et al.*, 2009, Jackson, (2015), Horswill & Escalante-Semerena, 2002, Conti *et al.*, 1997), we propose that Lys588 in the A10 region of PrpE is the catalytic residue for the adenylate-forming half-reaction.

The active site of PrpE in the thioester-forming conformation is sandwiched between the N-domain and the C-domain, as shown in the structure of PrpE in complex with AMP, acrylate and CoA (Fig. 4D, E). PrpE forms a pantetheine binding tunnel for the binding of the



pantetheine group of CoA (Fig. 4D). The pantetheine group of CoA is disordered based on the electron density. Though the exact location of the thiol arm of CoA can not be identified in our structure, structural alignment of PrpE and CoA bound acetyl-CoA synthetase (PDB code: 2P2F) shows that the trends of the thiol arms of CoAs in these two enzymes are similar, suggesting that the trend of the thiol arm of CoA in our structure is right (Fig S4). In addition, the electron density map indicates that acrylate takes a double-conformation in the structure, implying that acrylate undergoes conformational changes during the reaction. A sequence alignment reveals that Gly502 in the A8 region is strictly conserved among PrpEs. (Fig. S3). In the PrpE complex, Gly502 is on a loop that follows the hinge between the N- and C-domains in the middle of the active site and borders the pantetheine tunnel (Fig. 4E). Gly502 interacts with acrylate existing in double conformation, and therefore, is probably an important residue involved in positioning acrylate. This hypothesis is supported by the Gly502 to proline mutation (dramatically enlarges the side chain) resulting in no detectable PrpE activity (Fig. 4C). Conversely, replacing Gly502 with alanine, an amino acid of similar size and properties, had little influence on the activity of PrpE. Furthermore, structural analysis suggests that residues Arg171, Arg493, Lys504, Lys533 and Glu563 have interactions with CoA or AMP (Fig. 4E). Mutations of these residues also significantly decreased the activity of PrpE (Fig. 4C), implying that these residues in PrpE are likely involved in the binding of the substrates (Fig. 4E).

Based on the structural and mutagenesis analyses above, we propose a mechanism for PrpE to catalyze acrylate into acryloyl-CoA. The reaction can be divided into two steps. In the first step, when ATP and acrylate bind to the active site, PrpE orientates to the adenylate-forming conformation in which the A10 region (contains Lys588) is located in the active site. Then, the carboxyl oxygen of acrylate attacks the  $\alpha$ -phosphate of ATP, and the P-O bond between the  $\alpha$ -phosphate and the  $\beta$ -phosphate is cleaved, leading to the formation of the P-O bond between the  $\alpha$ -phosphate and the acrylate carboxyl oxygen and the formation of the adenylate intermediate acryloyl-AMP (Fig. 6A). In this step, the carboxyl oxygen of acrylate serves as the nucleophilic base that provides electrons, and the  $\beta$ -phosphate serves as the Brønsted acid that gains electrons. During the reaction, Lys588 helps to position the phosphoryl groups of ATP and to increase the acidity and the electrophilicity of the phosphorus. In the second step,

the C-domain undergoes a rotation, and PrpE re-orientates to the thioester-forming conformation in which the A8 region containing Gly502 is relocated into the active site. This reorientation forms a pantetheine binding tunnel for CoA. The thiol group of the incoming CoA functions as a nucleophile to launch an attack on the carbonyl group of the acryloyl-AMP intermediate. Along with the cleavage of the C-O bond between acrylate and AMP, the S-C bond between acrylate and CoA is formed (Fig. 6B), leading to the formation of the final product, acryloyl-CoA. In this step, Gly502 helps to form the pantetheine tunnel for CoA and to stabilize the intermediate. Thus, we illustrate the catalytic mechanism of PrpE to catalyze acrylate into acryloyl-CoA.

#### **The catalytic mechanism of AcuI for acryloyl-CoA reduction**

AcuI belongs to the MDR family. Enzymes in this family require NADPH as a cofactor to catalyze the reduction reaction (Persson *et al.*, 2008). The structure of AcuI in complex with NADPH shows that NADPH is located in the active site of AcuI (Fig. 5A, B), suggesting that NADPH is the cofactor for AcuI catalysis, similar to other enzymes in the MDR family (Khare *et al.*, 2015).

A previous study suggested that the substrate of MDR family enzymes should bind near the NADPH C4 hydride donor and that the reductase should provide a proton donor (amino acid or water molecule) in the reaction process (Khare *et al.*, 2015). Sequence alignments combined with the structural analysis of AcuI suggest that six hydrophilic residues (Asn43, Tyr44, Lys45, Thr133, Ser272 and Arg323) around the nicotinamide group of NADPH in AcuI may be involved in the catalytic reaction and provide the proton (Fig. S2). We performed site-directed mutagenesis on each of these hydrophilic residues. The N43A, Y44A, K45A, T133A, and S272A mutants showed activities similar to wild type AcuI (Fig. 5C). However, an R323A substitution dramatically decreased the AcuI activity (Fig. 5C), suggesting that Arg323 is probably a key residue for catalysis. To confirm this, further mutations at Arg323 were created. When Arg323 was mutated to lysine, a similar basic residue, the activity of AcuI was almost unaffected (Fig. 5C). However, when Arg323 was mutated to isoleucine, which is more hydrophobic, the activity of AcuI was almost completely abolished. These data suggest that Arg323 may participate in electron transfer and provide the proton in the catalytic process of AcuI. In addition, water may serve as the proton donor,

because a water molecule is only 4.4 Å from the NADPH-C4.

Based on previous studies on NADPH-dependent reductases (Matsumoto *et al.*, 2013, Schiebel *et al.*, 2014, Kubota *et al.*, 2011) and our structural and mutagenesis analyses, we propose a catalytic mechanism of AcuI for acryloyl-CoA reduction (Fig. 6C). In the reaction, NADPH acts as a reducing agent. When NADPH and acryloyl-CoA are bound in the active site, the reduction reaction proceeds via an attack from the nicotinamide-C4 pro-S-hydride on the substrate's C3 carbon. Then, the redundant electron is transferred to the carbonyl oxygen of acryloyl-CoA and forms an enolate intermediate. Subsequently, the unstable enolate intermediate moves its electron to a water molecule (or Arg323), resulting in the formation of the final product propionate-CoA, which is less toxic than acryloyl-CoA (Fig. 6C).

#### **An effective detoxification system for acrylate catabolism in DMSP-catabolizing Roseobacters**

Since intracellular acrylate and its metabolism to acryloyl-CoA are potentially harmful, microorganisms, especially DMSP-degrading bacteria, need a system to swiftly metabolise and detoxify these metabolites. The upregulation of *acul* in response to acrylate and/or DMSP by Roseobacters and some other bacteria (Sullivan *et al.*, 2011, Todd *et al.*, 2012) provides a possible mechanism to prevent the accumulation of acrylate and importantly acryloyl-CoA. To test whether a detoxification system also functions in DMSP-metabolizing Roseobacters, we investigated the  $K_m$  values of DMSP lyases, DmdA, PrpEs and AcuIs reported and studied in this work (Table 1).

As detailed above, DMSP cleavage by DMSP lyases produces DMS and acrylate or 3HP (DddD). It has been proposed that the DMSP demethylation pathway can also lead to the production of acrylate (Kiene & Taylor, 1988), something supported by the fact that the demethylation gene *dmdA* is co-transcribed with *acul* in DSS-3 and their transcription is enhanced by acrylate (Todd *et al.*, 2012). Furthermore, there are hypothetical pathways predicting that 3HP can be converted into acrylate or acryloyl-CoA (Asao & Alber, 2013). In some marine environments, acrylate itself can be utilized as a sole carbon source by marine bacteria (Tapiolas *et al.*, 2010). Intracellular acrylate, whatever its source, is further transformed by PrpEs into highly toxic acryloyl-CoA, which is then transformed by AcuIs into propionyl-CoA and this product is finally metabolized in the TCA cycle (Fig. 7). In this

pathway, DmdAs and most of the known bacterial DMSP lyases have high  $K_m$  values (4.5-81.9 mM) (Table 1). Although the exact  $K_m$  value of DddD to DMSP is not available, it has been suggested that the DMSP lyase DddD, which generates 3HP as a co-product with DMS and not acrylate, also has a relatively high  $K_m$  (Curson *et al.*, 2011b, Alcolombri *et al.*, 2014). An exception is DddY, a periplasmic DMSP lyase that is not found in Roseobacters (Table 1) (Curson *et al.*, 2011b, Alcolombri *et al.*, 2014). However, different from the DmdAs and DMSP lyases, AcuIs have extremely low  $K_m$  values (1.1-2.8  $\mu$ M) (Table 1). This indicates that the substrate affinities of DmdAs and DMSP lyases are low and the substrate affinities of AcuIs are very high.

This phenomenon may have physiological importance. DMSP catabolizing bacteria, including many Roseobacters, are known to concentrate DMSP to mM intracellular levels compared to nM environmental concentrations, likely through BCCT- and ABC-family transport systems (Fig. 7) (Sun *et al.*, 2016, Reisch *et al.*, 2013). Such high intracellular DMSP concentrations are proposed to function in osmoregulation and oxidative stress amelioration (Curson *et al.*, 2011b) in addition to providing a source of carbon, sulfur and energy through its catabolism via the demethylation or the cleavage pathways. The lower substrate affinities of DmdAs and DMSP lyases enable the bacteria to maintain a high intracellular concentration of DMSP (mM) allowing potential physiological benefits in, e.g., osmoprotection. In contrast, because acryloyl-CoA is highly toxic, the high affinity of AcuI is vital for the maintenance of a very low and safe concentration of this metabolite in the cells. This reflects an effective detoxification system for DMSP and acrylate metabolism adopted by DMSP-metabolizing Roseobacters to protect their cells. This detoxification system, potentially in concert with the upregulation of *acul* in response to raised acrylate or DMSP concentrations, is likely sufficient to achieve the goal of beneficial DMSP accumulation and the rapid metabolism of toxic acrylate and acryloyl-CoA.

#### **Wider relevance of our findings on AcuI and PrpE**

BLASTP results against the NCBI nr database showed that homologs to PrpE and AcuI are present in a very wide range of marine and terrestrial organisms. There are >6000 sequences homologous to AcuI and >5000 sequences homologous to PrpE (identity to AcuI/PrpE of DSS-3 >45%), spanning wide-ranging bacteria (proteobacteria-actinobacteria) and eukaryotes.

These enzymes are most widely distributed in bacteria. Presently there are at least three sequenced eukaryotes containing both *prpE* and *acul* (*Capitella teleta*: 54%/53% identity to DSS-3 AcuI/PrpE, *Drosophila eugracilis*: 52%/47% identity to DSS-3 AcuI/PrpE and *Trichuris trichiura*: 53%/45% to DSS-3 AcuI/PrpE).

The abundance of AcuI and PrpE in wide ranging organisms and environments together with the fact that acrylate and/or acryloyl-CoA is probably produced by metabolism of substances other than DMSP, such as lactate (Baldwin *et al.*, 1965, Kuchta & Abeles, 1985, Seeliger *et al.*, 2002), propionate (Sato *et al.*, 1999), beta-alanine (Herrmann *et al.*, 2005) and glucose (Zhou *et al.*, 2011), suggests that many other organisms probably utilize a similar detoxification system to allow metabolism and prevent accumulation of potentially toxic metabolites. Thus, the suggested detoxification system may be extended to other organisms and is likely relevant to many other metabolic processes and environments beyond DMSP catabolism in marine environments.

## **Experimental procedures**

### **Bacterial strains and growth conditions**

DSS-3, DFL 12 and ITI\_1157 were all purchased from the Leibniz Institute DSMZ-German Collection of Microorganisms and Cell Cultures and were cultured in the DSMZ rich media 974 (DSS-3) or 514 (DFL 12 and ITI\_1157) at 30°C (DSS-3) or 40°C (ITI\_1157) for 2 days before genome extraction. The *E. coli* strains DH5 $\alpha$  and BL21(DE3) were all grown in Luria–Bertani medium at 37°C.

### **Gene cloning, point mutation creation, protein expression and purification**

Genes were cloned from the genomes of DSS-3, DFL 12 and ITI\_1157 and overexpressed in *E. coli* BL21(DE3) cells using the pET-22b vector that contains a His-tag for purification (Novagen, America). All point mutations were introduced using the QuikChange® mutagenesis kit (Agilent, America). Recombinant and mutant proteins were purified with Ni<sup>2+</sup>-NTA resin (Qiagen, Germany), followed by anion exchange chromatography fractionation on a Source 15Q column and gel filtration on a Superdex G200 column (GE Health-care, America). The MW standards were bought from General Electric Company, America.

### Real-time qPCR analysis

Bacteria were cultured in 2216E medium (Becton, Dickinson and Company, America) at 30°C (DSS-3 and DFL12) or 40°C (ITI\_1157) to an OD<sub>600</sub> of 0.8. Then, ITI\_1157 and DFL 12 were induced by 5 mM DMSP or 2 mM acrylate, respectively. For DSS-3, 0.5 mM DMSP or 0.5 mM acrylate was used because we found that higher concentrations of DMSP or acrylate result in a reduction in the growth rate of DSS-3. Total RNA was extracted using the RNeasy® Mini Kit (QIAGEN, America) according to the manufacturer's instructions after 1 hour's induction. The extracted RNA was subsequently reverse-transcribed using the Prime-Script™ RT Reagent Kit with gDNA Eraser (TaKaRa, Japan), and then qPCR was performed using a Light Cycler II 480 System (Roche, Switzerland) following the instructions of SYBR® Premix Ex Taq™ (TaKaRa, Japan).

### Enzyme assays

For the PrpE enzyme assay, purified recombinant PrpE enzymes (0.5 μM) from DSS-3, DFL 12 and ITI1157 were incubated with 0.5 mM acrylate, 0.5 mM CoA, 0.5 mM ATP, 5 mM MgCl<sub>2</sub>, 100 mM Tris/HCl (pH 8.0). The reaction was performed at the optimal temperature (40°C) and pH (8.0) (Fig. S7) for 30 min, and was stopped by adding 10% hydrochloric acid. The control assay had the same reaction system except that PrpE was not added. The enzymatic activity of PrpE was measured by determining the production of acryloyl-CoA using high performance liquid chromatography (HPLC). Analyses were performed using a C<sub>18</sub> column (Waters, America) with a linear gradient of 1–20% acetonitrile in 20 mM ammonium acetate (pH 2.8) over 15 min at 260 nm.

The enzymatic activity of AcuI was measured by determining the production of propionate-CoA. Analyses were performed using a C<sub>18</sub> column (Waters, America) with a linear gradient of 1-20% acetonitrile in 20 mM ammonium acetate (pH 2.8) over 15 min at 260 nm. The enzyme assay mixture contained 0.5 mM acrylate, 0.5 mM CoA, 0.5 mM ATP, 5 mM MgCl<sub>2</sub>, 100 mM Tris/HCl (pH 8.0), 0.5 μM purified PrpE and 0.5 μM purified AcuI. The reaction was performed at 40°C and pH 8.0 for 30 min, and was stopped by adding 10% hydrochloric acid. The control assay had the same reaction system except that AcuI was not added. The optimal temperature and pH of PrpE (40°C and pH 8.0) were used because PrpE was the rate limiting enzyme in the reaction of AcuI assay and the optimal temperature and

pH of AcuI were unable to determine due to the lack of purified acryloyl-CoA.

#### **Crystallization and data collection**

PrpE from DFL 12 and AcuI from DSS-3 were crystallized at 20°C using the sitting drop vapor diffusion method (the ratio of protein to precipitant was 1:1). The purified proteins were concentrated to 10 mg ml<sup>-1</sup> in 10 mM Tris-HCl (pH 8.0) and 100 mM NaCl. PrpE was mixed with AMP, acrylate and CoA at a molar ratio of 1:5:5:5. AcuI was mixed with NADPH at a molar ratio of 1:5. All of the mixtures were incubated at 0°C for 15 min. PrpE complex crystals were obtained in a buffer containing 1.8 M ammonium sulfate, 0.1 M BIS-TRIS, pH 6.5, and 2% polyethylene glycol (PEG) monomethyl ether 550. The crystals of Apo-AcuI and AcuI in complex with NADPH were both obtained in the buffer containing 0.1 M Bis-Tris propane, 20% PEG 3350 and 0.2 M NaBr. Precipitant with 15% glycerol was used as cryoprotection buffer and the crystals were frozen by liquid nitrogen. The X-ray diffraction data were collected on the BL17U1 beam line at the Shanghai Synchrotron Radiation Facility using the detector ADSC Quantum 315r. The initial diffraction datasets were processed by HKL2000 (Ducruix A, 1999). Data collection statistics are shown in Table S1.

#### **Structure determination and refinement**

The obtained crystals of PrpE belonged to the C121 space group; the obtained crystals of AcuI belonged to the P22121 space group. The first one and the last two residues are not shown in the structure of PrpE. The electron densities between residues 241-245 and residues 543-550 of PrpE are unclear and discontinuous. In addition, the RSRZ scores of Arg585, Ser586, Gly587, Pro602, Trp603, Pro606, Ala613, Pro169 and Pro612 of PrpE are also a little high, which may result from the low quality of the densities. The phases were determined using the molecular replacement method (EMPR) (Adams *et al.*, 2002) using the CCP4 program Phaser (Potterton *et al.*, 2003). PrpE used acetyl-CoA synthetase (PDB code: 1PG4) and AcuI used YhdH (PDB code: 1O8C) as the search model. The refinement was done by Phenix (Adams *et al.*, 2002) and Coot (Emsley & Cowtan, 2004) alternately, and the quality of the final model is summarized in Table S1. All of the structural figures were processed using the program PyMOL (<http://www.pymol.org/>).

#### **Bioinformatics**

BLAST was used to perform similarity searches through the NCBI BLAST webpage interface

(<http://www.ncbi.nlm.nih.gov/BLAST/>). Clustal W was used to do multiple sequence alignments (<http://www.genome.jp/tools/clustalw/>).

### **Circular dichroism (CD) spectroscopy**

The CD spectra were collected from 250 nm to 200 nm at a scan speed of 200 nm min<sup>-1</sup> with a path length of 0.1 cm on a J-810 spectropolarimeter (Jasco, Japan). The final concentration of the proteins was 10 μM in 10 mM Tris-HCl (pH 8.0) and 100 mM NaCl.

### **Accession numbers**

The structures of apo-AcuI, AcuI in complex with NADPH and PrpE in complex with AMP, acrylate and CoA were deposited in the Protein Data Bank under the accession codes 5GXF, 5GXE and 5GXD, respectively

### **Acknowledgements**

We thank Andrew WB Johnston for his helpful suggestions for this work and thank the staff of BL19U1 and BL17U1 beamline (Wang *et al.*, 2016) at National Center for Protein Sciences Shanghai and Shanghai Synchrotron Radiation Facility, Shanghai, People's Republic of China, for assistance during data collection. This work was supported by the National Science Foundation of China (grants 31630012, 31290230 and 31290231), the Program of Shandong for Taishan Scholars (TS20090803), the National Postdoctoral Program for Innovative Talents (BX201600095, BX201700145) and Natural Environment Research Council (NERC) grants in the UK (NE/P012671, NE/N002385 and NE/M004449).

### **References**

- Adams, P.D., R.W. Grosse-Kunstleve, L.W. Hung, T.R. Ioerger, A.J. McCoy, N.W. Moriarty *et al.*, (2002) PHENIX: building new software for automated crystallographic structure determination. *Acta Crystallographica Section D-Biological Crystallography* **58**: 1948-1954.
- Alcolombri, U., P. Laurino, P. Lara-Astiaso, A. Vardi & D.S. Tawfik, (2014) DddD is a CoA-transferase/lyase producing dimethyl sulfide in the marine environment. *Biochemistry* **53**: 5473-5475.
- Archer, S.D., C.E. Widdicombe, G.A. Tarran, A.P. Rees & P.H. Burkill, (2001) Production and



turnover of particulate dimethylsulphoniopropionate during a coccolithophore bloom in the northern North Sea. *Aquat Microb Ecol* **24**: 225-241.

Asao, M. & B.E. Alber, (2013) Acrylyl-Coenzyme A Reductase, an Enzyme Involved in the Assimilation of 3-Hydroxypropionate by *Rhodobacter sphaeroides*. *J Bacteriol* **195**: 4716-4725.

Baldwin, R.L., W.A. Wood & R.S. Emery, (1965) Lactate Metabolism by *Peptostreptococcus Elsdenii*: Evidence for Lactyl Coenzyme a Dehydrase. *BBA* **97**: 202-213.

Biebl, H., M. Allgaier, B.J. Tindall, M. Koblizek, H. Lunsdorf, R. Pukall *et al.*, (2005) *Dinoroseobacter shibae* gen. nov., sp. nov., a new aerobic phototrophic bacterium isolated from dinoflagellates. *Int J Syst Evol Microbiol* **55**: 1089-1096.

Brummett, A.E. & M. Dey, (2016) New Mechanistic Insight from Substrate- and Product-Bound Structures of the Metal-Dependent Dimethylsulfonypropionate Lyase DddQ. *Biochemistry* **55**: 6162-6174.

Brummett, A.E., N.J. Schnicker, A. Crider, J.D. Todd, & M. Dey, (2015) Biochemical, kinetic, and spectroscopic characterization of *Ruegeria pomeroyi* DddW--a mononuclear iron-dependent DMSP lyase. *PLoS One* **10**:e0127288.

Clayden, J., G.N., S. Warren, P. Wothers (2001) Organic Chemistry. Oxford: Oxford University Press.

Conti, E., T. Stachelhaus, M.A. Marahiel & P. Brick, (1997) Structural basis for the activation of phenylalanine in the non-ribosomal biosynthesis of gramicidin S. *EMBO J* **16**: 4174-4183.

Curson, A.R., O.J. Burns, S. Voget, R. Daniel, J.D. Todd, K. McInnis *et al.*, (2014) Screening of metagenomic and genomic libraries reveals three classes of bacterial enzymes that overcome the toxicity of acrylate. *Plos One* **9**: e97660.

Curson, A.R., J. Liu, A.B. Martinez, R.T. Green, Y. Chan, O. Carrion *et. al.*, (2017) Dimethylsulfonypropionate biosynthesis in marine bacteria and identification of the key gene in this process. *Nat microbiol* **2**: 17009.

Curson, A.R., M.J. Sullivan, J.D. Todd & A.W. Johnston, (2011a) DddY, a periplasmic dimethylsulfonypropionate lyase found in taxonomically diverse species of Proteobacteria. *Isme J* **5**: 1191-1200.

- Curson, A.R., J.D. Todd, M.J. Sullivan & A.W. Johnston, (2011b) Catabolism of dimethylsulphoniopropionate: microorganisms, enzymes and genes. *Nat Rev Microbiol* **9**: 849-859
- Ducruix, A., R. Giegé, (1999) Crystallization of Nucleic Acids and Proteins (Oxford Univ Press, New York), 2nd Ed.
- Elssner, T., C. Engemann, K. Baumgart & H.P. Kleber, (2001) Involvement of coenzyme A esters and two new enzymes, an enoyl-CoA hydratase and a CoA-transferase, in the hydration of crotonobetaine to L-carnitine by *Escherichia coli*. *Biochemistry* **40**: 11140-11148.
- Emsley, P. & K. Cowtan, (2004) Coot: model-building tools for molecular graphics. *Acta Crystallogr D Biol Crystallogr* **60**: 2126-2132.
- Gulick, A.M., X. Lu & D.D. Mariano, (2004) Crystal structure of 4-chlorobenzoate:CoA ligase/synthetase in the unliganded and aryl substrate-bound states. *Biochemistry* **43**: 8670-8679.
- Gulick, A.M., V.J. Starai, A.R. Horswill, K.M. Homick & J.C. Escalante-Semerena, (2003) The 1.75 Å crystal structure of acetyl-CoA synthetase bound to adenosine-5'-propylphosphate and coenzyme A. *Biochemistry* **42**: 2866-2873.
- Herrmann, G., T. Selmer, H.J. Jessen, R.R. Gokarn, O. Selifonova, S.J. Gort & W. Buckel, (2005) Two beta-alanyl-CoA:ammonia lyases in *Clostridium propionicum*. *FEBS J* **272**: 813-821.
- Hisanaga, Y., H. Ago, N. Nakagawa, K. Hamada, K. Ida, M. Yamamoto *et al.*, (2004) Structural basis of the substrate-specific two-step catalysis of long chain fatty acyl-CoA synthetase dimer. *J Biol Chem* **279**: 31717-31726.
- Horswill, A.R. & J.C. Escalante-Semerena, (2002) Characterization of the propionyl-CoA synthetase (PrpE) enzyme of *Salmonella enterica*: residue Lys592 is required for propionyl-AMP synthesis. *Biochemistry* **41**: 2379-2387.
- Jackson, D.R., S.S. Tu, M. Nguyen, J.F. Barajas, A.J. Schaub, & D. Krug, (2015) Structural insights into anthranilate priming during type ii polyketide biosynthesis. *Acs Chem Biol*. **11**: 95-103
- Jogl, G. & L. Tong, (2004) Crystal structure of yeast acetyl-coenzyme A synthetase in

- complex with AMP. *Biochemistry* **43**: 1425-1431.
- Khare, D., W.A. Hale, A. Tripathi, L. Gu, D.H. Sherman, W.H. Gerwick *et al.* (2015) Structural Basis for Cyclopropanation by a Unique Enoyl-Acyl Carrier Protein Reductase. *Structure* **23**: 2213-2223.
- Kiene, R.P., L.J. Linn and J.A. Bruton, (2000) New and important roles for DMSP in marine microbial communities. *J Sea Res* **43(3)**:209-224.
- Kiene, R.P. & B.F. Taylor, (1988) Demethylation of dimethylsulfoniopropionate and production of thiols in anoxic marine sediments. *Appl Environ Microbiol* **54**: 2208-2212.
- Kirkwood, M., J.D. Todd, K.L. Rypien & A.W.B. Johnston, (2010) The opportunistic coral pathogen *Aspergillus sydowii* contains *dddP* and makes dimethyl sulfide from dimethylsulfoniopropionate. *ISME J* **4**: 147-150.
- Kochan, G., E.S. Pilka, F.V. Delft, U. Oppermann & W.W. Yue, (2009) Structural snapshots for the conformation-dependent catalysis by human medium-chain acyl-coenzyme A synthetase ACSM2A. *J Mol Biol* **388**: 997-1008.
- Kubota, K., K. Nagata, M. Okai, K. Miyazono, W. Soemphol, J. Ohtsuka *et al.*, (2011) The crystal structure of l-sorbose reductase from *Gluconobacter frateurii* complexed with NADPH and l-sorbose. *J Mol Biol* **407**: 543-555.
- Kuchta, R.D. & R.H. Abeles, (1985) Lactate reduction in *Clostridium propionicum*. Purification and properties of lactyl-CoA dehydratase. *J Biol Chem* **260**: 13181-13189.
- Li, C.Y., T.D. Wei, S.H. Zhang, X.L. Chen, X. Gao, P. Wang *et al.*, (2014a) Molecular insight into bacterial cleavage of oceanic dimethylsulfoniopropionate into dimethyl sulfide. *PNAS* **111**: 1026-1031.
- Li, C.Y., X.L. Chen, B.B. Xie, H.N. Su, Q.L. Qin & Y.Z. Zhang, (2014b) Reply to Tawfik *et al.*: DddQ is a dimethylsulfoniopropionate lyase involved in dimethylsulfoniopropionate catabolism in marine bacterial cells. *PNAS* **111**: E2080.
- Malmstrom, R.R., R.P. Kiene & D.L. Kirchman, (2004) Identification and enumeration of bacteria assimilating dimethylsulfoniopropionate (DMSP) in the North Atlantic and Gulf of Mexico. *Limnol Oceanogr* **49**: 597-606.

- Marahiel, M.A., T. Stachelhaus & H.D. Mootz, (1997) Modular Peptide Synthetases Involved in Nonribosomal Peptide Synthesis. *Chem Rev* **97**: 2651-2674.
- Marc J.E.C., B. Maarel, S.V. Bergeijk, A.F.V. Werkhoven, A.M. Laverman, W. G. Meijer, *et al.* (1996) Cleavage of dimethylsulfonylpropionate and reduction of acrylate by *desulfovibrio acrylicus* sp. nov. *Arch Microbiol* **166(2)**, 109-115.
- Matsumoto, K., Y. Tanaka, T. Watanabe, R. Motohashi, K. Ikeda, K. Tobitani *et al.* (2013) Directed evolution and structural analysis of NADPH-dependent Acetoacetyl Coenzyme A (Acetoacetyl-CoA) reductase from *Ralstonia eutropha* reveals two mutations responsible for enhanced kinetics. *Appl Environ Microbiol* **79**: 6134-6139.
- Persson, B., J. Hedlund & H. Jornvall, (2008) Medium- and short-chain dehydrogenase/reductase gene and protein families : the MDR superfamily. *Cell Mol Life Sci* **65**: 3879-3894.
- Petursdottir, S.K. & J.K. Kristjansson, (1997) *Silicibacter lacuscaerulensis* gen. nov., sp. nov., a mesophilic moderately halophilic bacterium characteristic of the Blue Lagoon geothermal lake in Iceland. *Extremophiles* **1**: 94-99.
- Potterton, E., P. Briggs, M. Turkenburg & E. Dodson, (2003) A graphical user interface to the CCP4 program suite. *Acta Crystallogr D Biol Crystallogr* **59**: 1131-1137.
- Rajashekhara E., K. Watanabe, (2004) Propionyl-coenzyme A synthetases of *Ralstonia solanacearum* and *Salmonella choleraesuis* display atypical kinetics. *FEBS Lett* **556**:143-147.
- Reger, A.S., J.M. Carney & A.M. Gulick, (2007) Biochemical and crystallographic analysis of substrate binding and conformational changes in acetyl-CoA synthetase. *Biochemistry* **46**: 6536-6546.
- Reisch, C.R., W.M. Crabb, S.M. Gifford, Q. Teng, M.J. Stoudemayer, M.A. Moran & W.B. Whitman, (2013) Metabolism of dimethylsulfonylpropionate by *Ruegeria pomeroyi* DSS-3. *Mol Microbiol* **89**: 774-791.
- Reisch, C.R., M.J. Stoudemayer, V.A. Varaljay, I.J. Amster, M.A. Moran & W.B. Whitman, (2011) Novel pathway for assimilation of dimethylsulfonylpropionate widespread in marine bacteria. *Nature* **473**: 208-211.
- Sato, K., Y. Nishina, C. Setoyama, R. Miura & K. Shiga, (1999) Unusually high standard

redox potential of acrylyl-CoA/propionyl-CoA couple among enoyl-CoA/acyl-CoA couples: a reason for the distinct metabolic pathway of propionyl-CoA from longer acyl-CoAs. *J Biochem* **126**: 668-675.

Schiebel, J., A. Chang, S. Shah, Y. Lu, L. Liu, P. Pan *et al.* (2014) Rational design of broad spectrum antibacterial activity based on a clinically relevant enoyl-acyl carrier protein (ACP) reductase inhibitor. *J Biol Chem* **289**: 15987-16005.

Schnicker, N.J., S.M. Silva, J.D. Todd & M. Dey, (2017) Structural and biochemical insights into dimethylsulfoniopropionate cleavage by cofactor-bound DddK from the prolific marine bacterium *Pelagibacter*. *Biochemistry* online.

Seeliger, S., P.H. Janssen & B. Schink, (2002) Energetics and kinetics of lactate fermentation to acetate and propionate via methylmalonyl-CoA or acrylyl-CoA. *FEMS Microbiol Lett* **211**: 65-70.

Seymour, J.R., R. Simo, T. Ahmed & R. Stocker, (2010) Chemoattraction to dimethylsulfoniopropionate throughout the marine microbial food web. *Science* **329**: 342-345.

Sievert, S.M., R.P. Kiene & H.N. Schulz-Vogt, (2007) The Sulfur Cycle. *Oceanography* **20**: 117-123.

Simo, R., S.D. Archer, C. Pedros-Alio, L. Gilpin & C.E. Stelfox-Widdicombe, (2002) Coupled dynamics of dimethylsulfoniopropionate and dimethylsulfide cycling and the microbial food web in surface waters of the North Atlantic. *Limnol Oceanogr* **47**: 53-61.

Souza, M.P.D., & D.C. Yoch, (1996) N-terminal amino acid sequences and comparison of DMSP lyases from *Pseudomonas doudehoffii*, and *Alcaligenes* strain M3A. *Estuaries*, **20**(2), 361-362.

Sullivan, M.J., A.R. Curson, N. Shearer, J.D. Todd, R.T. Green & A.W. Johnston, (2011) Unusual regulation of a leaderless operon involved in the catabolism of dimethylsulfoniopropionate in *Rhodobacter sphaeroides*. *Plos One* **6**: e15972.

Sulzenbacher, G., V. Roig-Zamboni, F. Pagot, S. Grisel, A. Salomoni, C. Valencia *et al.* (2004) Structure of *Escherichia coli* YhdH, a putative quinone oxidoreductase. *Acta Crystallogr D Biol Crystallogr* **60**: 1855-1862.

- Sun, J., J.D. Todd, J.C. Thrash, Y. Qian, M.C. Qian, B. Temperton *et al.* (2016) The abundant marine bacterium *Pelagibacter* simultaneously catabolizes dimethylsulfoniopropionate to the gases dimethyl sulfide and methanethiol. *Nat Microbio* **1**: 16065.
- Tapiolas, D.M., C.A. Motti, P. Holloway & S.G. Boyle, (2010) High levels of acrylate in the Great Barrier Reef coral *Acropora millepora*. *Coral Reefs* **29**: 621-625.
- Todd, J.D., A.R. Curson, N. Nikolaidou-Katsaraidou, C.A. Brearley, N.J. Watmough, Y. Chan *et al.*, (2010) Molecular dissection of bacterial acrylate catabolism--unexpected links with dimethylsulfoniopropionate catabolism and dimethyl sulfide production. *Environ Microbiol* **12**: 327-343.
- Todd, J.D., A.R. Curson, M.J. Sullivan, M. Kirkwood & A.W. Johnston, (2012) The *Ruegeria pomeroyi acul* gene has a role in DMSP catabolism and resembles yhdH of *E. coli* and other bacteria in conferring resistance to acrylate. *PLoS One* **7**: e35947.
- Vandecandelaere, I., O. Nercessian, E. Segart, W. Achouak, M. Faimali & P. Vandamme, (2008) *Ruegeria scottomollicae* sp. nov., *Int J Syst Evol Microbiol*. **58**: 2726-2733.
- Wang, P., X.L. Chen, C.Y. Li, X. Gao, D.Y. Zhu, B.B. Xie *et al.* (2015) Structural and molecular basis for the novel catalytic mechanism and evolution of DddP, an abundant peptidase-like bacterial Dimethylsulfoniopropionate lyase: a new enzyme from an old fold. *Molecular microbiology* **98**: 289-301.
- Wang, Z., Q. Pan, L. Yang, H. Zhou, C. Xu, F. Yu *et al.*, (2016) Automatic crystal centring procedure at the SSRF macromolecular crystallography beamline. *J Synchrotron Radiat* **23**: 1323-1332.
- Yoch, D.C., (2002) Dimethylsulfoniopropionate: its sources, role in the marine food web, and biological degradation to dimethylsulfide. *Appl Environ Microbiol* **68**: 5804-5815.
- Zhou, F.L., Y.G. Zhang, R.B. Zhang, W. Liu & M. Xian, (2011) Expression and characterization of a novel propionyl-CoA dehydrogenase gene from *Candida rugosa* in *Pichia pastoris*. *Appl Biochem Biotec* **165**: 1770-1778.

### Figure legends

**Fig. 1. Two different pathways for acrylate metabolism in two DMSP-catabolizing bacteria.** (A) The *AcuN-AcuK* pathway in *Halomonas* HTNK1 (Todd *et al.*, 2010). (B) The *PrpE-AcuI* pathway in *Ruegeria pomeroyi* DSS-3 (Reisch *et al.*, 2013).

**Fig. 2. Functional analysis of the genes involved in acrylate metabolism from Roseobacters DSS-3, DFL 12 and ITI\_1157.** (A) RT-qPCR assay of the transcriptions of *prpE*, *acuI*, *acuN* and *acuK* in DSS-3, DFL-12 and ITI\_1157 exposed to either DMSP or acrylate. DSS-3, DFL-12 and ITI\_1157 without induction were used as controls. The folds were calculated by comparing to the controls. (B) Detection of acryloyl-CoA ligase activity of *PrpE* from DSS-3 and ITI\_1157 via HPLC. The acryloyl-CoA peak is indicated with a red arrow. (C) Detection of acryloyl-CoA reductase activity of *AcuI* from DSS-3 and ITI\_1157 via HPLC. The acryloyl-CoA and propionate-CoA peaks are indicated with red arrows.

**Fig. 3. Overall structures of *PrpE* from DFL 12 and *AcuI* from DSS-3.** (A) Analysis of the forms of *PrpE* and *AcuI* in solution by gel filtration. The molecular weight of *PrpE* is 70 kDa. It is a monomer in solution. The molecular weight of *AcuI* is 35 kDa. It is a dimer in solution. (B) Overall structure of *PrpE*. It contains an N-domain and a C-domain. The N-domain contains two parallel  $\beta$ -sheets of seven strands (sheet 1 and sheet 2) and an antiparallel  $\beta$ -sheet (sheet 3) of five strands. The C-domain forms a three-stranded  $\beta$ -sheet (sheet 4) with helices on its face. The ligands (AMP, CoA and acrylate) are shown in the view of spheres. The active center is labeled out with an orange circle. (C) Overall structure of *AcuI* dimer. The dimer is locked by two antiparallel strand-strand interactions. The ligands (NADPH) are shown in the view of spheres. The proposed binding sites of acryloyl-CoA are marked with orange circles. (D) Overall structure of *AcuI* monomer. It contains a typical rossmann fold. NADPH is shown as magenta sticks.

**Fig. 4. Analyses of the *PrpE* structure and the important residues in the active site.** (A) Cartoon view of the overall structure of *PrpE* in the thioester-forming conformation. The conserved A8 region is inside the active center and the A10 region is out of the active center. The residues in the middle of the N-domain and C-domain are shown in the stick view and coloured in purple. (B) Cartoon view of the overall structure of *PrpE* in the adenylate-forming conformation. The conserved A10 region is inside the active center and the A8 region is out of

the active center. (C) Activities of the PrpE variants. (D) Electrostatic surface view of PrpE in its thioester-forming conformation. AMP, acrylate and CoA are shown in the active site. (E) Conserved hydrophilic residues in the active site. Residues are shown in yellow sticks. The  $2F_o - F_c$  densities for AMP, acrylate and CoA are contoured in light blue, green and orange at  $1.5 \sigma$ . The distances are labeled in orange.

**Fig. 5. Analyses of the AcuI structure and the important residues in the active site.** (A) Electrostatic surface view of AcuI. The AcuI dimer forms two active sites, and two NADPH molecules are in the active sites. (B) Conserved hydrophilic residues in the active sites. The residues are shown in orange sticks. The simulated-annealing omit map for NADPH is contoured in gray 70 at  $2.0 \sigma$ . (C) Activities of the AcuI variants.

**Fig. 6. A proposed catalytic mechanism for acrylate degradation via PrpE and AcuI in Roseobacters.** The catalytic process consists of three steps, two catalyzed by PrpE and one catalyzed by AcuI. The first step is the adenylate-forming step in which acrylate is added to AMP to form acrylate-AMP. In this step, the carboxyl oxygen of acrylate acts as a nucleophilic base. Lys588 helps to position the ATP phosphoryl groups and to increase the acidity and the electrophilicity of the phosphorus. The second step is the thioester-forming step in which the AMP of acrylate-AMP is released and acryloyl-CoA is formed. This step happens after the C-domain of PrpE rotates approximately  $140^\circ$  and the A8 region rotates into the active site. The last step is the acryloyl-CoA reduction step in which acryloyl-CoA is reduced and propionate-CoA is formed. In this step, NADPH serves as the reducing agent and a water molecule acts as an electron acceptor.

**Fig. 7. An effective detoxification system for acrylate catabolism in DMSP-catabolizing Roseobacters.** DMSP can be cleaved extracellularly or intracellularly. When it is metabolized intracellularly, there is an effective detoxification system helps Roseobacters to protect their cells. The detoxification system may be extended to other organisms and metabolisms. The  $K_m$  values of the enzymes are marked in brown, the toxicities of acrylate and acryloyl-CoA are marked in blue, and the functions of DMSP are marked in orange.



Table 1  $K_m$  values of DMSP<sup>1</sup> lyases, PrpE and AcuI

Organism	Gene	Substrates	Products	Apparent $K_m$ (mM)	
<i>Pelagibacter</i> HTCC1062	<i>dmdA</i>	DMSP	MMPA, Methyl	$13 \pm 2.0$	Sun <i>et al.</i> (Sun <i>et al.</i> , 2016)
<i>R. pomeroyi</i> str. DSS-3	<i>dmdA</i>	DMSP	MMPA, Methyl	$5.4 \pm 2.3$	Reisch <i>et al.</i> (Reisch <i>et al.</i> , 2011)
<i>R. pomeroyi</i> str. DSS-3	<i>dddP</i>	DMSP	Acrylate, DMS <sup>2</sup> ,	$21.6 \pm 5.8$	This study
<i>Roseovarius</i> <i>nubinihibens</i> str. ISM	<i>dddP</i>	DMSP	Acrylate, DMS	$13.8 \pm 5.5$	Kirkwood <i>et al.</i> (Kirkwood <i>et al.</i> , 2010)
<i>R.lacuscaerulen</i> <i>sis</i> str. ITI-1157	<i>dddP</i>	DMSP	Acrylate, DMS	$17.1 \pm 0.98$	Wang <i>et al.</i> (Wang <i>et al.</i> , 2015)
<i>R. pomeroyi</i> str. DSS-3	<i>dddQ</i>	DMSP	Acrylate, DMS	$18.1 \pm 1.0$	This study
<i>R.lacuscaerulen</i> <i>sis</i> str. ITI-1157	<i>dddQ</i>	DMSP	Acrylate, DMS	$21.5 \pm 6.8$ (Zn <sup>2+</sup> )	Li <i>et al.</i> (Li <i>et al.</i> , 2014b)
<i>R.lacuscaerulen</i> <i>sis</i> str. ITI-1157	<i>dddQ</i>	DMSP	Acrylate, DMS	$39.1 \pm 6.1$ (Fe <sup>3+</sup> ) $14.3 \pm 3.3$ (Fe <sup>2+</sup> )	Brummett <i>et al.</i> (Brummett & Dey, 2016)
<i>R. pomeroyi</i> str. DSS-3	<i>dddW</i>	DMSP	Acrylate, DMS	$8.68 \pm 0.73$ (Fe <sup>2+</sup> ) $4.50 \pm 0.75$ (Mn <sup>2+</sup> )	Brummett <i>et al.</i> (Brummett <i>et al.</i> , 2015)

<i>P. HTCC1062</i>	<i>dddK</i>	DMSP	Acrylate, DMS	81.9 ± 17.2 5.13 ± 0.4 (Ni <sup>2+</sup> )	Sun, <i>et al.</i> (Sun <i>et al.</i> , 2016) Schnicker, <i>et al.</i> (Schnicker <i>et al.</i> , 2017)
<i>A. faecalis</i>	<i>dddY</i>	DMSP	Acrylate, DMS	2.34	Souza <i>et al.</i> (Souza, 1996)
<i>Desulfovibrio acrylicus</i>	<i>dddY</i>	DMSP	Acrylate DMS	0.4	Marc <i>et al.</i> (Marc <i>et al.</i> , 1996)
<i>D. shibae</i> str. DFL 12	<i>prpE</i>	Acrylate, CoA, ATP	Acrylyl -CoA	2.14 ± 0.3	This study
<i>R. pomeroyi</i> str. DSS-3	<i>prpE</i>	Acrylate, CoA, ATP	Acrylyl -CoA	3.08 ± 0.15	This study
<i>R. lacuscaerulen sis</i> str. ITI-1157	<i>prpE</i>	Acrylate, CoA, ATP	Acrylyl -CoA	3.62 ± 0.2	This study
<i>Ralstonia solanacearum</i>	<i>prpE</i>	Acrylate, CoA, ATP	Acrylyl -CoA	1.0 ± 0.1	Horswill <i>et al.</i> (Horswill & Escalante-Semer ena, 2002)
<i>S. choleraesuis</i>	<i>prpE</i>	Acrylate, CoA, ATP	Acrylyl -CoA	1.3 ± 0.07	Horswill <i>et al.</i> (Horswill & Escalante-Semer ena, 2002)
<i>S. enterica</i>	<i>prpE</i>	Acrylate,	Acrylyl	0.279±	Rajashekhara <i>et</i>

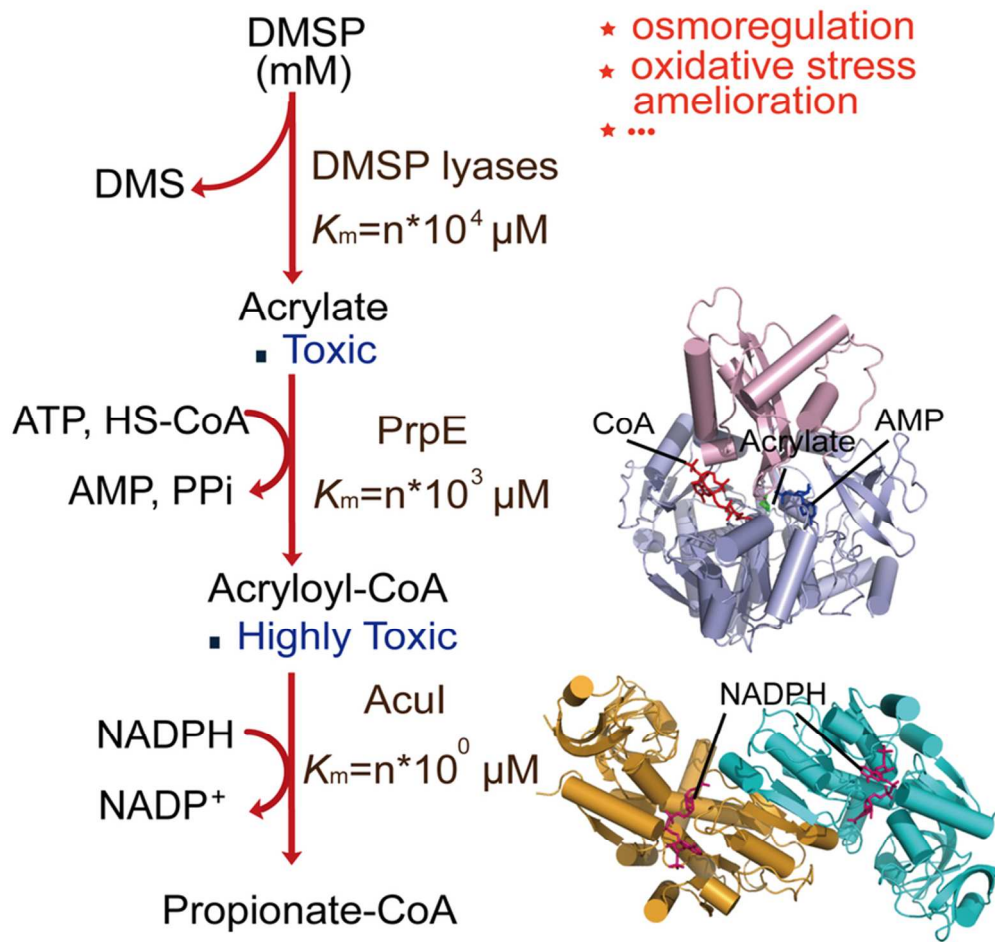
		CoA,	-CoA	0.014	<i>al.</i>
		ATP			(Rajashekhara & Watanabe, 2004)
<i>Rhodobacter</i>	<i>acul</i>	Acrylyl	Propionyl	≤ 1.5	Asao <i>et al.</i>
<i>sphaeroides</i>		-CoA,	-CoA		(Asao & Alber, 2013)
2.4.1		NADPH			
<i>R. pomeroyi</i>	<i>acul</i>	Acrylyl	Propionyl	≤ 2.8	Asao <i>et al.</i>
str. DSS-3		-CoA,	-CoA		(Asao & Alber, 2013)
		NADPH			
<i>E. coli</i> K-12	<i>acul</i>	Acrylyl	Propionyl	≤ 1.1	Asao <i>et al.</i>
substrain		-CoA,	-CoA		(Asao & Alber, 2013)
MG1655		NADPH			

<sup>1</sup> DMSP, dimethylsulfoniopropionate.

<sup>2</sup> DMS, dimethyl sulfide.

Accepted Article

Dimethylsulfoniopropionate (DMSP) cleavage, yielding dimethyl sulfide (DMS) and acrylate, is an important step in global sulfur cycling. Since acrylate is toxic to cells, it is important to understand how organisms utilize and detoxify acrylate. Through molecular and structural analyses, we provide the molecular mechanism for acrylate metabolism and detoxification in DMSP-catabolizing Roseobacters and suggest an effective detoxification system which is likely relevant to many metabolic processes and environments beyond DMSP catabolism in Roseobacters.



75x71mm (300 x 300 DPI)

Acce

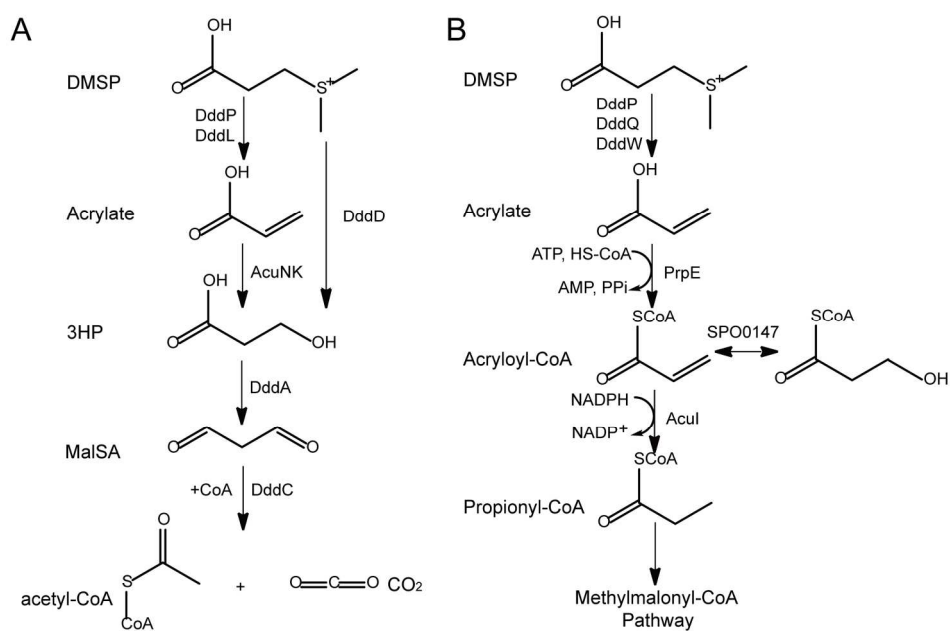


Fig. 1. Two different pathways for acrylate metabolism in two DMSP-catabolizing bacteria. (A) The AcuN-AcuK pathway in *Halomonas* HTNK1 (Todd et al., 2010). (B) The PrpE-AcuI pathway in *Ruegeria pomeroyi* DSS-3 (Reisch et al., 2013).

169x108mm (300 x 300 DPI)

Accept

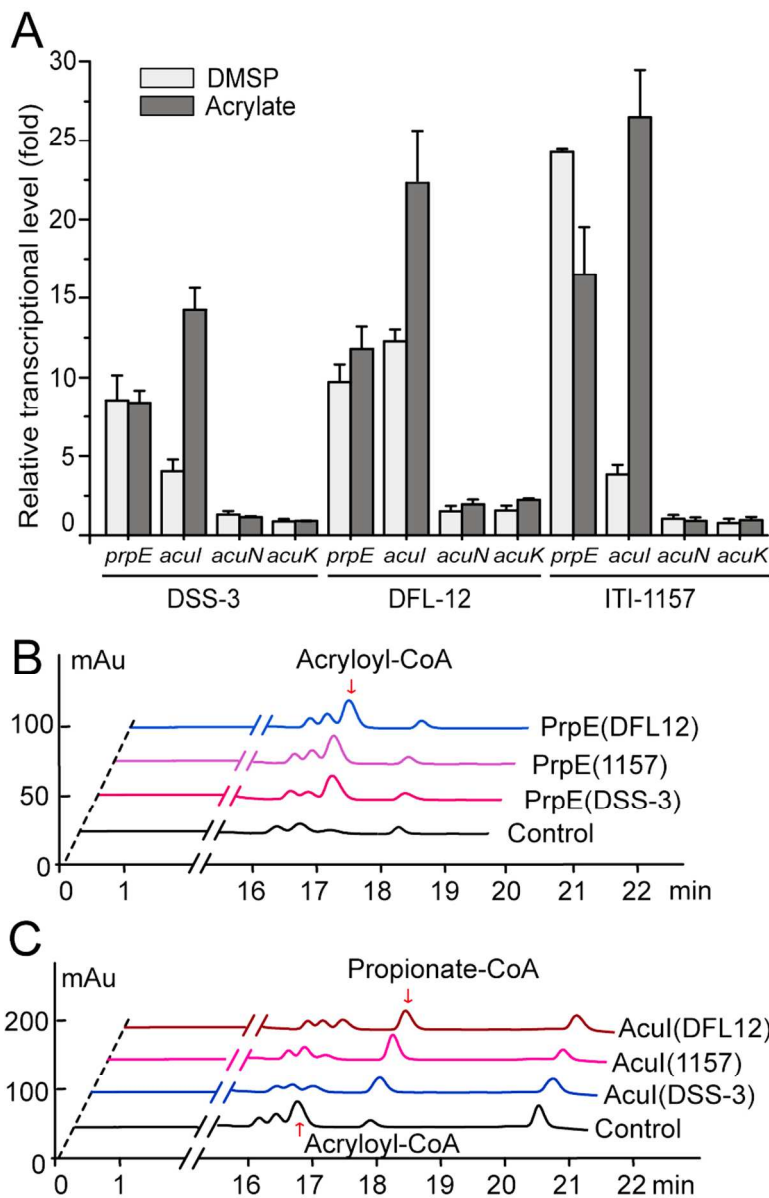


Fig. 2. Functional analysis of the genes involved in acrylate metabolism from Roseobacters DSS-3, DFL 12 and ITI\_1157. (A) RT-qPCR assay of the transcriptions of *prpE*, *acul*, *acuN* and *acuK* in DSS-3, DFL-12 and ITI\_1157 exposed to either DMSP or acrylate. DSS-3, DFL-12 and ITI\_1157 without induction were used as controls. The folds were calculated by comparing to the controls. (B) Detection of acryloyl-CoA ligase activity of PrpE from DSS-3 and ITI\_1157 via HPLC. The acryloyl-CoA peak is indicated with a red arrow. (C) Detection of acryloyl-CoA reductase activity of AcuI from DSS-3 and ITI\_1157 via HPLC. The acryloyl-CoA and propionate-CoA peaks are indicated with red arrows.

80x125mm (300 x 300 DPI)

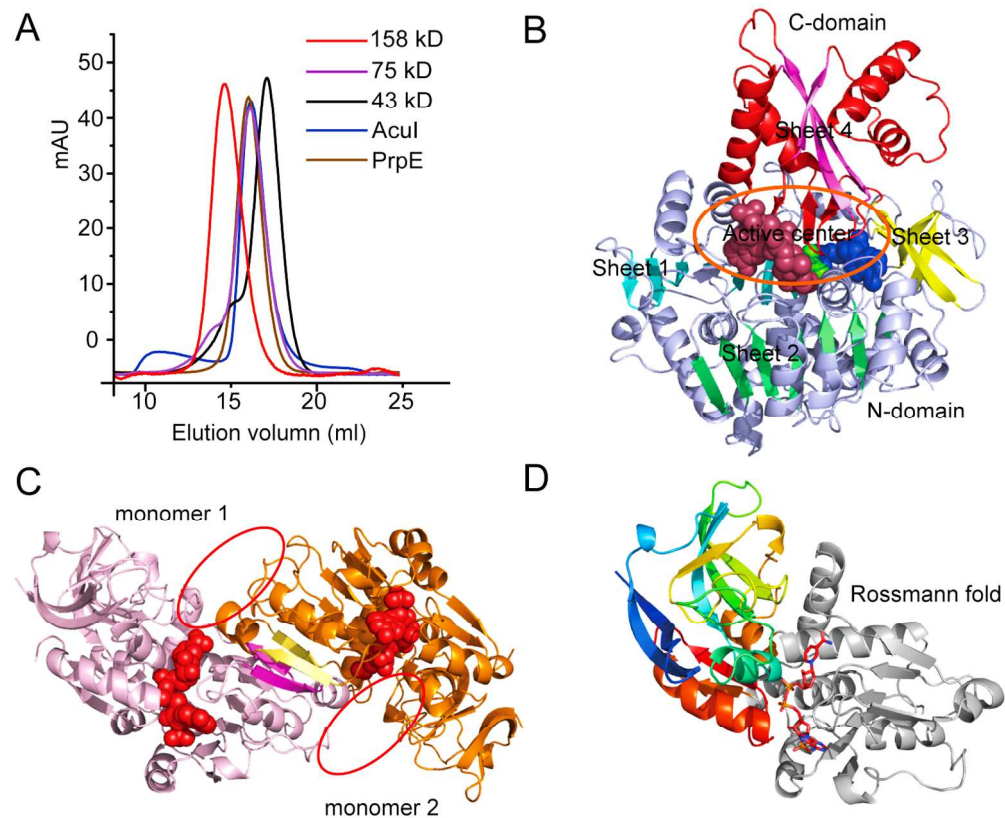


Fig. 3. Overall structures of PrpE from DFL 12 and AcuI from DSS-3. (A) Analysis of the forms of PrpE and AcuI in solution by gel filtration. The molecular weight of PrpE is 70 kDa. It is a monomer in solution. The molecular weight of AcuI is 35 kDa. It is a dimer in solution. (B) Overall structure of PrpE. It contains an N-domain and a C-domain. The N-domain contains two parallel  $\beta$ -sheets of seven strands (sheet 1 and sheet 2) and an antiparallel  $\beta$ -sheet (sheet 3) of five strands. The C-domain forms a three-stranded  $\beta$ -sheet (sheet 4) with helices on its face. The ligands (AMP, CoA and acrylate) are shown in the view of spheres. The active center is labeled out with an orange circle. (C) Overall structure of AcuI dimer. The dimer is locked by two antiparallel strand-strand interactions. The ligands (NADPH) are shown in the view of spheres. The proposed binding sites of acryloyl-CoA are mark with orange circles. (D) Overall structure of AcuI monomer. It contains a typical rossmann fold. NADPH is shown as magenta sticks.

139x115mm (300 x 300 DPI)

ACC



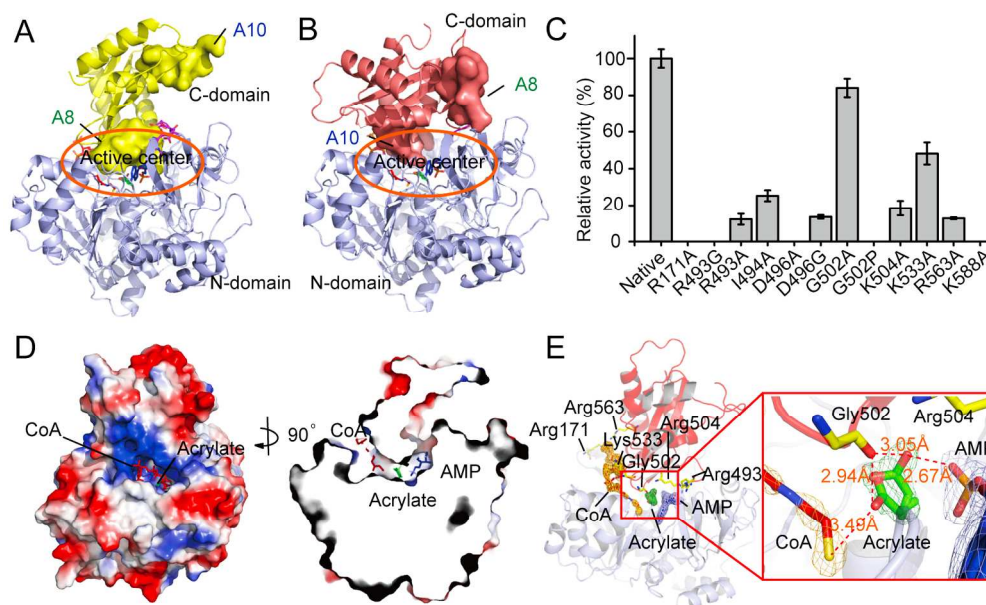


Fig. 4. Analyses of the PrpE structure and the important residues in the active site. (A) Cartoon view of the overall structure of PrpE in the thioester-forming conformation. The conserved A8 region is inside the active center and the A10 region is out of the active center. The residues in the middle of the N-domain and C-domain are shown in the stick view and coloured in purple. (B) Cartoon view of the overall structure of PrpE in the adenylate-forming conformation. The conserved A10 region is inside the active center and the A8 region is out of the active center. (C) Activities of the PrpE variants. (D) Electrostatic surface view of PrpE in its thioester-forming conformation. AMP, acrylate and CoA are shown in the active site. (E) Conserved hydrophilic residues in the active site. Residues are shown in yellow sticks. The 2Fo-Fc densities for AMP, acrylate and CoA are contoured in light blue, green and orange at 1.5  $\sigma$ . The distances are labeled in orange.

169x104mm (300 x 300 DPI)

Accel

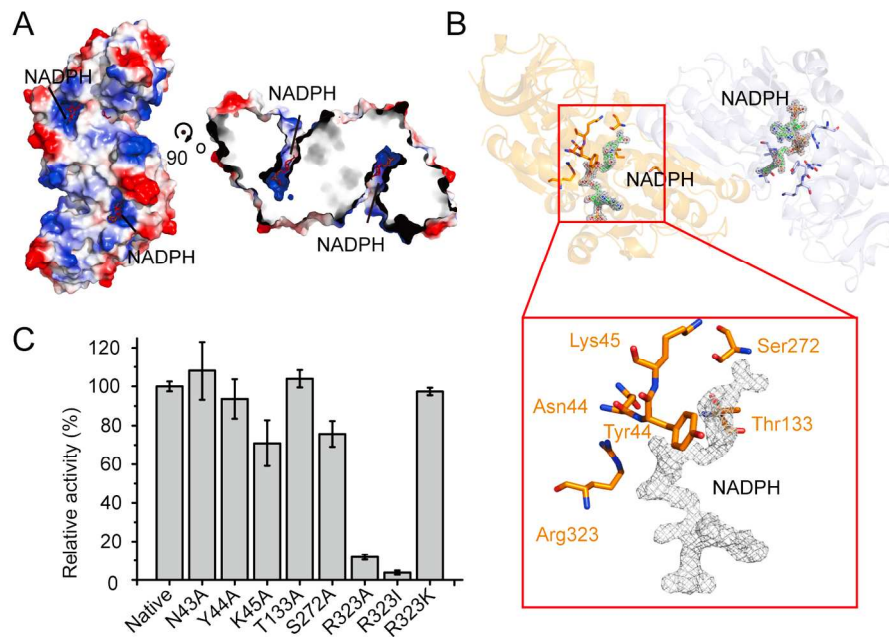


Fig. 5. Analyses of the AcuI structure and the important residues in the active site. (A) Electrostatic surface view of AcuI. The AcuI dimer forms two active sites, and two NADPH molecules are in the active sites. (B) Conserved hydrophilic residues in the active sites. The residues are shown in orange sticks. The simulated-annealing omit map for NADPH is contoured in gray 70 at  $2.0 \sigma$ . (C) Activities of the AcuI variants.

162x110mm (300 x 300 DPI)

Accepted

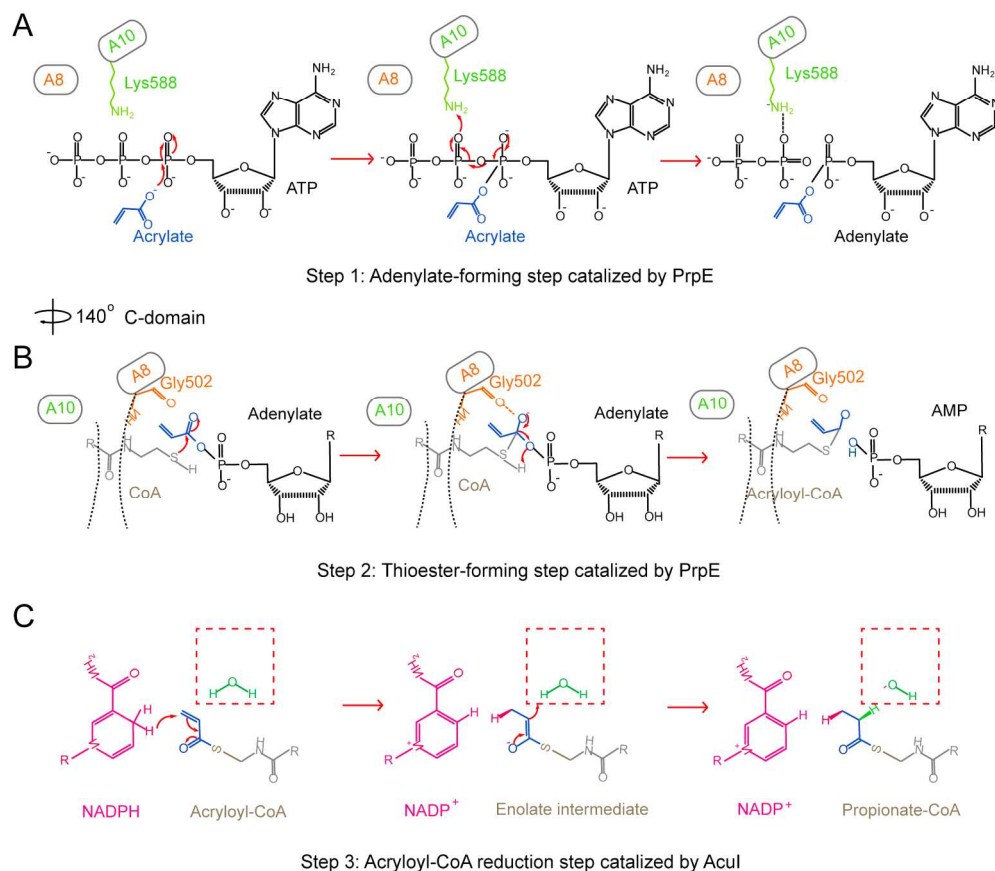


Fig. 6. A proposed catalytic mechanism for acrylate degradation via PrpE and AcuI in Roseobacters. The catalytic process consists of three steps, two catalyzed by PrpE and one catalyzed by AcuI. The first step is the adenylate-forming step in which acrylate is added to AMP to form acrylate-AMP. In this step, the carboxyl oxygen of acrylate acts as a nucleophilic base. Lys588 helps to position the ATP phosphoryl groups and to increase the acidity and the electrophilicity of the phosphorus. The second step is the thioester-forming step in which the AMP of acrylate-AMP is released and acryloyl-CoA is formed. This step happens after the C-domain of PrpE rotates approximately  $140^\circ$  and the A8 region rotates into the active site. The last step is the acryloyl-CoA reduction step in which acryloyl-CoA is reduced and propionate-CoA is formed. In this step, NADPH serves as the reducing agent and a water molecule acts as an electron acceptor.

169x151mm (300 x 300 DPI)

AcuI

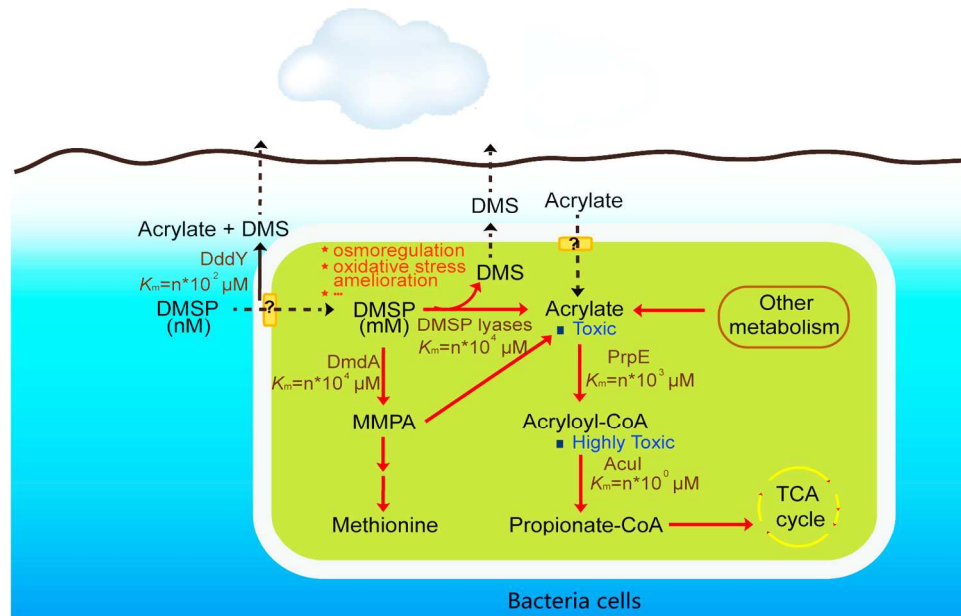


Fig. 7. An effective detoxification system for acrylate catabolism in DMSP-catabolizing Roseobacters. DMSP can be cleaved extracellularly or intracellularly. When it is metabolized intracellularly, there is an effective detoxification system helps Roseobacters to protect their cells. The detoxification system may be extended to other organisms and metabolisms. The  $K_m$  values of the enzymes are marked in brown, the toxicities of acrylate and acryloyl-CoA are marked in blue, and the functions of DMSP are marked in orange.

152x98mm (300 x 300 DPI)

Accept